Biomedical Signal Processing and Control 31 (2017) 339–349

Contents lists available at ScienceDirect

Biomedical Signal Processing and Control

journal homepage: www.elsevier.com/locate/bspc

Empirical Mode Decomposition-based filtering for fatigue induced hand tremor in laparoscopic manipulation

Sourav Chandra [a], Mitsuhiro Hayashibe [b], Asokan Thondiyath [a,*]

[a] Department of Engineering Design, Indian Institute of Technology Madras, Chennai 600036, India
[b] INRIA Sophia-Antipolis and LIRMM, Université de Montpellier, 34095 Montpellier Cedex 5, France

ARTICLE INFO

Article history:
Received 22 December 2015
Received in revised form 20 July 2016
Accepted 26 August 2016
Available online 8 September 2016

Keywords:
Muscle fatigue
Hand tremor filtering
Robot assisted surgery
Empirical Mode Decomposition
Kullback–Leibler Divergence

ABSTRACT

Fatigue induced hand tremor (FIT) is an unavoidable phenomenon, which substantially limits the accuracy of the surgical manipulation for long duration laparoscopic surgeries. Filtering intended motion from tremor is a challenging task as the properties of tremor change with increasing muscle fatigue levels. Muscle fatigue induced hand tremor has highly nonlinear and nonstationary characteristics that need a filtering strategy different from the conventional filters. Empirical Mode Decomposition (EMD) based filters have become popular in the recent past for its enhanced nonlinear signal handling capability. EMD based filtering strategy is case specific in nature as the EMD does not have any general analytical formulation unlike other (Kernel based) popular filtering techniques. In this work, we have addressed the tremor filtering issue with the help of EMD and the probability distribution characteristics analysis of Intrinsic Mode Functions (IMF) of the tremulous laparoscopic tool trajectory. A modified distribution asymmetry measure was employed to find out the threshold IMF for reconstruction of tremor free motion at different fatigue levels. In order to find the robustness of the proposed technique, the compensation strategy has been tested extensively on synthetic signal and experimentally acquired signals. Filtering threshold at different fatigue levels was also demonstrated for various subjects. Despite the time-varying properties of tremor, the proposed filtering strategy substantiates its efficacy to diminish the effect of tremor which was not possible by the conventional fixed cut-off filtering techniques.

1. Introduction

Minimally invasive surgery has its unique advantages over the conventional surgery for patients, as it offers reduced incision, quick recovery, and reduced hospital stay [1]. However, it is challenging from the surgeons' perspective as they have to manipulate specialized tool for prolonged timespan in an uncomfortable posture [2]. Hand tremor severely limits the quality of laparoscopic manipulation in minimally invasive surgery (MIS), where highly accurate movements are of primary interest [3,4]. Fatigue induced tremor (FIT) is a high frequency oscillating movement which adheres to the low frequency intended hand motion [5]. FIT frequency vary between 4Hz and 25Hz, depending upon the muscle fatigue level [6,5]. In Manual Laparoscopic Surgery (MLS) the surgical tool is directly manipulated by the doctor, and in Robot Assisted Laparoscopic Surgical (RALS) systems the surgeons' hand movement is reproduced by a slave manipulator inside the patient body. As the RALS has an intermediate controller, it is possible to employ a tremor compensation system for an accurate reproduction of intended surgical motion [7]. Implementation of tremor compensation is challenging in RALS since the characteristics of FIT changes significantly with the course of time with the increasing muscle fatigue [5,8,6].

The tremor signal is comprised of both deterministic and stochastic components [9,5], as a consequence the probability distribution changes with time. This makes the task of FIT compensation difficult for a filtering technique with the conventional Fourier based approach having a fixed *a priory basis*. A linear, fixed cut-off filtering with conventional Finite Impulse Response (FIR) or Infinite Impulse Response (IIR) structure based filters are incompetent to filter out the tremor from the intended motion as the tremor characteristics changes dynamically [10]. Even though wavelet based filtering can handle non-stationarity of signal to some extent, it fundamentally relies upon varying window *Fourier Spectral Analysis*, which essentially is a linear method [11]. Moreover, the wavelet thresholding process presumes that signal magnitude is significantly higher than the noise magnitude which is grossly discarded

* Corresponding author.
E-mail addresses: ed11d004@smail.iitm.ac.in (S. Chandra), Mitsuhiro.Hayashibe@inria.fr (M. Hayashibe), asok@iitm.ac.in (A. Thondiyath).

http://dx.doi.org/10.1016/j.bspc.2016.08.025
1746-8094/

in case of tremor affected surgical manipulation [10]. Essentially, hand tremor compensation requires a signal processing scheme that can handle FIT without the assumption of linearity and stationarity.

EMD is a well celebrated method which can address the above mentioned issues of FIT compensation in an elegant manner [9]. It is a signal decomposition technique which works essentially in time domain, and sequentially decomposes the signal into various sub components known as IMF [12]. Though EMD has been extensively used for analysing hand movements [13,14], it has never been employed as a tool for minimizing the effect of FIT in dynamic scenarios where the tremor characteristics changes at different fatigue level. In this work EMD is used primarily as a tremor compensatory tool, in order to reduce the effect of tremor in laparoscopic tool manipulation (LTM) in dominant axis of tremor [8]. As the name suggests, EMD is a data driven decomposition process that depends upon numerical values of the signal. Since EMD assign the basis posteriorly, the temporal variation of the signal defines the number of basis; these basis are known as Intrinsic Mode Function (IMF) of the signal [12]. As a consequence, the high frequency activities are preserved with intact superior details in different IMFs without the prior assumption of linearity and stationarity [15,16]. The original signal can be reconstructed by summing up all the IMFs along with its residue. Partial cumulative sum of the IMFs makes the EMD based framework suitable for the current filtering scenario. Filtering capability of such strategies already has been established, although setting up the accumulation limit is unique and depends upon the nature of the application [17].

The objective of the present work is reconstruction of the FIT free intended laparoscopic manipulation trajectory by deciding a limiting reconstruction threshold on the IMFs. The idea of partial reconstruction was tried previously by a number of research groups [10,18], and the criteria for selection of reconstruction threshold in different scenarios were studied. Some of them are distribution dissimilarity based i.e. Kullback–Leibller Divergence (KLD) [19], and pattern recognition based approach, i.e. Hausdorff Distance [20], whereas few other works relied upon inferential statistics based criterion to find the limit [10]. Despite of its directional dependency, KLD is well accepted for its direct relation with the distribution mean, while the directional dependencies needs to be taken care of [19,20]. The critical factor of the current problem is the poor availability of information about the intended motion of the surgeon which varies with time, and relating fatigue level information for reducing tremor effects in a plausible manner. Primary backbone of the proposed approach is that the intended motion of the LTM is contributed by the higher order IMFs which have a lower frequency [15] and the lower order IMFs containing the high frequency components. It was assumed that the intended motion can occupy higher frequency modes depending upon the frequency content of LTM, i.e. a sudden fast movement in the case of a delicate suturing task performed in MLS is very common.

Muscle fatigue levels give the physiological perspective of tremor as the tremor changes due to the inability of producing sufficient torque with increasing fatigue in the associated muscle [21]. In this work, hand tremor at different fatigue level has been analyzed for all the experimental data. Assessment of muscle fatigue was carried out using the Mean Frequency (MF) analysis of Surface ElectroMyoGraphy (SEMG) signal recorded from the concerned prime mover muscle [22]. With the increasing fatigue level, MF drops down due to decreased conduction velocity of the neural excitation and increased synchronization of motor unit firing [23,6]. In this paper, we have demonstrated that the EMD based filtering works efficiently even though the tremor characteristics changes with increased muscle fatigue. The reconstruction thresholds for filtering were selected based on the Symmetric Kullback–Leibller Divergence (SKLD). Variation of the reconstruction threshold depending upon the varying tremor is demonstrated with hand tremor-like synthetic signal and the real tremor signal as well. Finally, the compensation strategy is verified with the experimentally acquired fatigue induced hand tremor data in laparoscopic manipulation.

2. Methods and conceptual framework

2.1. EMD based tremor filtering strategy

A significant advantage of employing EMD is its inherent adaptive nature, as the method resolves the signal to a set of posteriori defined basis (IMF), that are essentially derived from the data itself [15]. The IMFs ($IMF_n(t)$), are generated sequentially through the shifting process under some pre-determined criteria [12]. After the EMD of the tremulous signal, the resulting IMFs contains different amplitude and frequency values while having a identical time scale ($t = [1 : T]$) for all of them [17]. In this sequential decomposition procedure the frequency content of the IMF decreases gradually to a minimum value in the final IMF. Resulting IMFs always ensure that in terms of frequency $IMF_{n+1}(t) < IMF_n(t)$. This property of IMF drives the proposed tremor filtering framework as shown in Fig. 1.

Contribution of additive high frequency FIT varies with the changing muscle fatigue levels at different experimental task epochs. MF variation of the SEMG signal signifies the change in fatigue level of the associated muscle. Selective accumulation of the resolved $IMF_n(t)$ leads to a low frequency intended motion at different muscle fatigue level. Selection of the threshold was accomplished at each fatigue level on the basis of the consecutive IMFs' probability distribution asymmetry.

Symmetric Kullback–Liebler Divergence (SKLD) values at each fatigue level were used to determine the threshold of the reconstruction of the tremor free signal at different experimental task epoch. SKLD differentiates the IMF from a stochastic perspective as discussed in Section 4.3. Here the SKLD was used for detecting the distribution dissimilarity among $IMF_n(t)$ and $IMF_{n+1}(t)$ for all n. Since it is not possible to have a reference tremor signal for using it as a conventional filter, unlike the previous attempts with synthetic signals [20,24], different threshold was found at different stage of increasing fatigue level. After the threshold selection, reconstruction of the tremor free signal was accomplished by partial accumulation with the threshold bounded IMFs. This hierarchical filtering approach experimentally exhibited an efficient means to reduce the effect of FIT in LTM.

2.2. Detection of tremulous movement using wearable inertial sensors

Tremor compensation framework described in Section 2.3 requires the detection of the tremulous movement in LTM which can be carried out in various ways (i.e. optically, magnetically, or using inertial sensors) [25,26]. In this work, the trajectory of the tremulous tool manoeuvering in the sagittal plane was recorded with wearable inertial sensors (tri-axial accelerometer) as in the line diagram shown in Fig. 2. An elbow rest was provided in order to create the experimental scenario similar to the RAS [27,28,26].

Here we have used an accelerometer based joint angle measurement, where sagittal plane movement of forearm and palm with the elbow rest can be modeled as an inverted pendulum [29]. This approach of limb pose detection is appropriate in current scenario because tracking of the tool gripping point using other method often is not easy in the case of laparoscopic tool movement [26]. In order to deal with the high frequency tremor, the data acquisition rate has to be considerably high, which can be easily achieved with the current approach of inertial motion based sensing.

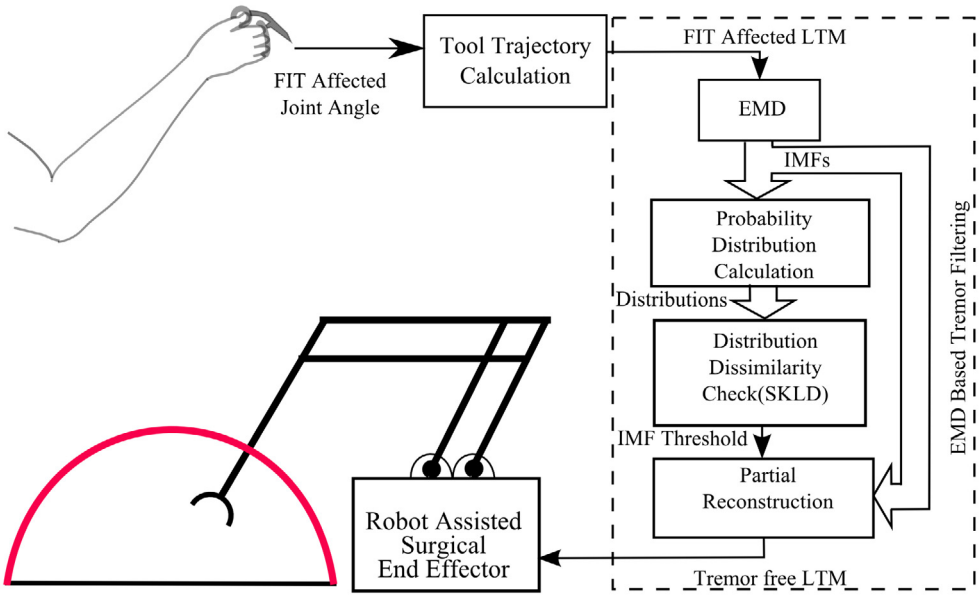

Fig. 1. EMD based fatigue induced tremor compensation strategy.

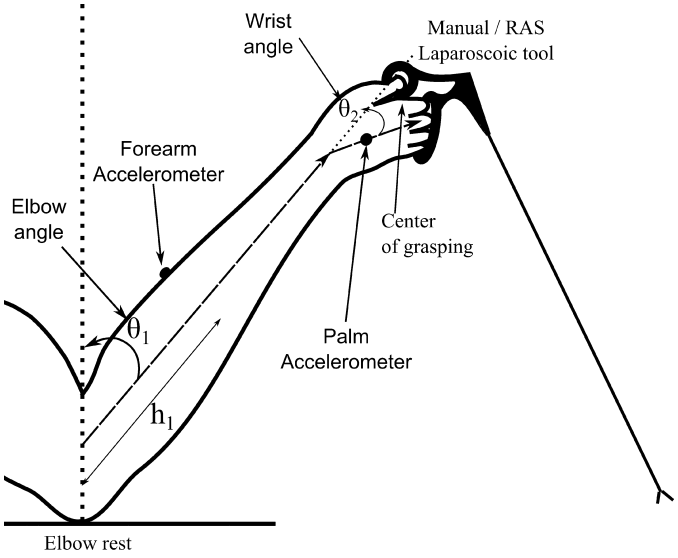

Fig. 2. Schematic representation of tool holding during LTM.

Furthermore, it gives a clear limb segment based idea of tremor, which is advantageous as the calculation of tremor sensing becomes a bottom up approach in current scenario. The initial tilt correction of the tri-axial accelerometers were performed at the beginning of the experiment.

The elbow angle can be found using the pendulum equation using the planar acceleration as:

$$a_1 = h_1\ddot{\theta}_1 - g\sin(\theta_1) \tag{1}$$

where a_1 is the forearm acceleration value in sagittal plane while performing LTM, h_1 is the distance to the forearm accelerometer from elbow joint, θ_1 is elbow angle in sagittal plane, and g is gravitational constant (= 9.81 m/s^2). The wrist angle in sagittal plane can be found with the extended formulation of (1), where forearm and palm movements are imposed as a planar inverted double pendulum as described in [29]. Here the joint angles were calculated while performing the experimental task. With the help of the measured joint angle, the forearm length and the palm length, a 2-R planar serial link forward kinematics can be employed to find the pose of the laparoscopic tool grasping point. Finally the values were fed to the EMD process for IMF decomposition.

2.3. EMD algorithm

Unlike the other signal decomposition methods (i.e. *Fourier*, *Gabor*, *Wavelet*), EMD is a time-domain decomposition process that works without the help of integral transformation. This numeric decomposition process starts with finding the maxima and minima of the tremor affected raw signal. A maxima $x_{max} = (x_{max1}, x_{max2}, \ldots, x_{max\,p})$ and minima $x_{min} = (x_{min1}, x_{min2}, \ldots, x_{min\,q})$ envelop-pair is generated using the detected points, where p and q are the number of maxima and minima. These points were used to generate the envelop pairs env_{max} and env_{min} employing a *Cubic Spline* interpolation method [30]. This was followed by calculation of envelop mean and the resulting data was investigated for the IMF properties. A resulting signal can be considered as an IMF if it matches with the following criteria [15]:

- Within the dataset timespan, the number of extrema and the number of zero crossing has to be either equal or differ at most by one. This property is the key factor to segregate the oscillatory modes starting from a higher frequency and gradually sliding down to a lower frequency.
- $env^t_{mean} = \frac{env^t_{\max} + env^t_{\min}}{2} = 0$, which essentially ensures that at any time instant (t) the mean of the two envelop values env_{mean} will be zero.

The EMD process can be summarized in the following steps

1. Selection of the hand tremor affected laparoscopic tool manipulation trajectory $x(t)$.
2. Identification of x_{max}, x_{min}.
3. Generating env_{max} and env_{min} by interpolating x_{max} and x_{min}.
4. Computation of the envelop mean as

$$env_{mean} = \frac{env^t_{\max} + env^t_{\min}}{2}.$$

5. Calculation of the intermediate signal based on the env_{mean} as $d(t) = x(t) - env_{mean}(t)$ and check $d(t)$ for the above mentioned IMF criteria.
6. If $d(t)$ satisfies the IMF criteria, $d(t)$ is deducted from $x(t)$ and saved as an IMF; the whole process reiterates with the residue. In case $d(t)$ does not meet the IMF criteria, it is again considered for the iteration.
7. The iteration continues until the residue ($res(t)$) meets the stopping criterion.

The stopping criterion was determined depending upon the information content of the signal. Standard Deviation (SD) is a common measure for such application where an IMF with a higher frequency will have a higher SD [31,10]. For our application the SD is given by (2) and limit was set at 0.2.

$$SD_i = \sum_{t=0}^{T} \frac{[d_i(t) - d_{i+1}(t)]^2}{d_i(t)^2} \tag{2}$$

where i denotes the number of IMF, and T is the time span of the signal after the final decomposition, the raw signal can be represented by a bunch of IMF along with the final residue. The IMFs are nearly orthogonal in nature [15]. The raw signal can be reconstructed by summing up the IMFs and the residue r(t) as:

$$x(t) = \sum_{i=1}^{n} IMF_i(t) + r(t) \tag{3}$$

The main idea of the tremor filtering is inspired from this reconstructability property of the IMFs. A complete reconstruction leads to the original raw signal, whereas a partial reconstruction leads to a resulting signal where some portions are filtered.

2.4. Reconstruction thresholding of IMF at different fatigue level

Tremor affected surgeons' movement can be represented as $x(t) = x_{in}(t) + x_{fi}(t) + x_{hf}(t)$, where $x_{in}(t)$ is the intended movement that does not change as an effect of fatigue, $x_{hf}(t)$ is the constant high frequency (≈30Hz) noise inherent to the human limb called systemic tremor [6] and $x_{fi}(t)$ is the fatigue induced tremor which changes depending upon the fatigue state of the muscle [5].

The objective of signal reconstruction is to recover an approximate of the signal $\hat{x}(t)$ from the IMFs of the original tremor affected signal $x(t)$. The partially reconstructed signal can be mathematically represented as

$$\hat{x}(t) = \sum_{i=m}^{n} IMF_i(t) + r(t) \tag{4}$$

where $m > 1$ and $r(t)$ is the residue.

The proposed filtering approach is asymptotic in nature as the value of the filtered signal was approximated within two best subsequent partial IMF terms, which enables us to find the bounds of the IMFs. Selection of the value m is crucial in (4) as the IMF contains two type of higher frequency. The high frequency *Gaussian Noise* $x_{hf}(t)$ stays almost constant, while the FIT $x_{fi}(t)$ varies with muscle fatigue level. Difference in two unknown signal with mixed components in it imposes a different distribution altogether. Though there are several methods to differentiate them, these are highly application specific [10,18]. Distribution asymmetry based separation of signals has been considered to be an efficient means of differentiating dissimilar signals [10], as discussed in the following section.

2.5. Selection criterion for reconstruction threshold

Selection of IMF threshold for reconstruction of the tremor free signal $\hat{x}(t)$ depends upon the dissimilarities among the IMFs. With the changing tremor characteristics, predominant high frequency tremor contribution gets shared by varying number of the lower order IMFs. Variation of IMF frequency content can be substantiated with the number of zero crossing of the consecutive IMFs, which defines the tremor content as well [16]. These dissimilarities signify varying amplitude and frequency of the IMFs [13,16], which get captured together in their probability distribution. Probability distribution of IMF_i can be calculated by superimposing a smooth distribution on their histogram using the kernel density estimation approach [20]. Bin size for the histogram calculation was kept fixed at 150 throughout the experiment.

In the current scenario dissimilarities between two consecutive IMFs are calculated with the help of a statistical measurement called Symmetric Kullback–Leibller Divergence (SKLD) [32]. For two distributions, having Probability Mass Function (PMF) as P_i and P_{i+1}, the Symmetric K–L Divergence (SKLD) between the two distribution is defined as

$$\text{SKLD}|_{P_i \to P_{i+1}} = \frac{1}{2}(\text{KLD}|_{P_i \to P_{i+1}} + \text{KLD}|_{P_{i+1} \to P_i}) \tag{5}$$

where

$$\text{KLD}|_{P_i \to P_{i+1}} = \int P_i(x) \cdot \log\left(\frac{P_i(x)}{P_{i+1}(x)}\right) dx \tag{6}$$

In case of discrete values, (6) can be approximated as

$$\text{KLD}|_{P_i \to P_{i+1}} = \sum_{\forall x} P_i(x) \cdot \log\left(\frac{P_i(x)}{P_{i+1}(x)}\right) \tag{7}$$

Significantly, even though the KLD has a directional dependency i.e. $\text{KLD}|_{P_i \to P_{i+1}} \neq \text{KLD}|_{P_{i+1} \to P_i}$, SKLD is resistant to directional asymmetry. There exists $n-1$ number of SKLD values for n number of IMFs as described in (3). The highest among the SKLD indicates to the IMF pairs which bears the maximum disparity among their distribution. The maximum SKLD value can be selected as a threshold for generating $\hat{x}(t)$ with the help of (4). So the value of m can be calculated as

$$m = \max(SKLD_i|_{\forall i}) \tag{8}$$

Value of m changes for the signal with the increased level of muscle fatigue, as the frequency content of the respective IMF changes with increased fatigue. In case the max(SKLD) is among the nth and $(n+1)$th IMF, it indicates that the highest difference is resulting from the addition of the $(n+1)$th IMF [10]. The IMF corresponding to the max(SKLD) was used as the $IMF_{threshold}$ and the lower order IMFs containing higher frequency (i.e. $IMF_n \leqslant IMF_{threshold}$) were discarded while reconstruction. At this point we hypothesize that this highest disparity was introduced due to the characteristic difference in tremor and intended motion as discussed in Section 2.4. The IMFs above this limit contributes to the low frequency intended motion whereas below this limit IMFs significantly contributes to tremor.

3. Experimental setup and subject details

3.1. Subjects and set up for the experiment

Volunteers of different age group has participated in the experiment (age: 34.07 ± 4.2 years). Among the total 16 subjects, 2 were highly skilled senior robotics/laparoscopic surgeons ($Y_{exp} > 10$), 6 were mid-level experienced ($Y_{exp} < 10$) and 8 novice. All the subjects were informed a priory about the experimental process and

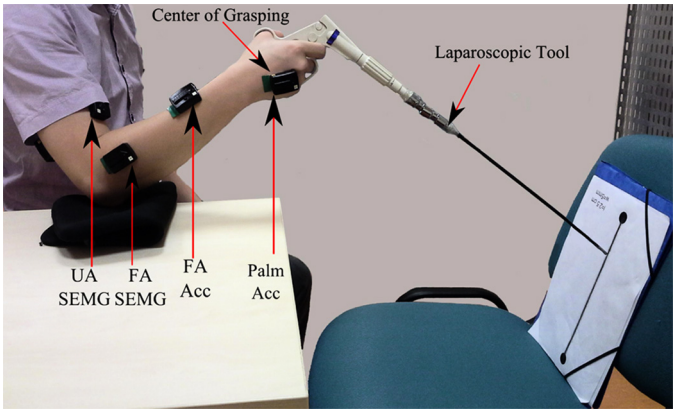

Fig. 3. Experimental setup for laparoscopic manipulation task, showing upper arm (UA) SEMG sensor, fore arm (FA) and palm accelerometer.

a written consent was taken from all the subjects. As the experimental set up and protocol involved human subject, we have followed *Helsinki Declaration* of 1975 (revised in 2000). The subjects were provided with sufficient amount of tool manoeuvering period in order to familiarize with the task before they actually start the experiment. This also helps to reduce the cognitive load for the assigned laparoscopic experimental manipulative task for the experiment. A laparoscopic grasper (*AutoSuture Endo Grasp*™) was used for the experimental task and the subjects were instructed to hold the laparoscopic grasper firmly with a palmar grasp while sitting in a comfortable posture with the elbow placed on arm rest [33,34], as shown in Fig. 3. For the instructed sagittal plane movement while holding the tool with a firm grip, the prime mover muscle for the fore arm is *Biceps Brachii* (BB), and for the palm, *Extensor Carpi Radialis Longus* (ECRL) and *Extensor Carpi Radialis Brevis* (ECRB). These superficial muscles are easily accessible, also the effect of fatigue is higher on the anterior muscle group which makes them fit for selection. Forward dynamics calculation of a serial manipulator ensures that the base joint of the manipulator requires highest torque, which has been investigated for human arm elbow wrist movements [35,5]. This makes the BB preferred for detecting effect of fatigue due to wrist and the elbow movement together. Throughout the experiment Surface ElectroMyoGraphy for the Non-Invasive Assessment of Muscles (SENIAM) standards were followed for acquiring SEMG signal.

A *Delsys TRIGNO*™ system was used to record the SEMG as well as the acceleration data for the forearm and the palm movement while the subjects were performing the sagittal plane laparoscopic movement. The amplified SEMG was sampled at 4 kHz, followed by a 4th order band pass filtering with a pass band 2–200 Hz before it was used for mean frequency calculation. The accelerometer ranges were selected to be 1.5 g with a sampling frequency 297 Hz. The accelerometer data was pre-processed with a high pass filter with a cut off set at 0.01 Hz before it was used for further calculation.

3.2. Experimental methods

The subjects were instructed to perform the LTM task in a comfortable sitting posture, an elbow rest was provided to make the experimental scenario similar to RAS [27]. The instructed tasks were (i) dynamic line tracking in sagittal plane and (ii) static holding of the laparoscopic tool. In Dynamic line tracking Task (DT), subjects were asked to traverse 25 cm long line drawn on a vertical plane, which is a common laparoscopic traversing length [25]. In the Static holding Task (ST), all the subjects were instructed to hold the tool at a given point without any movement. Each of the task epoch was performed for a duration of 40 s and repeated with a 10 min gap between each iteration. Six such iterations were performed, resembling a total activity of an hour, capturing the effects of fatigue in submaximal muscle contraction activities [6]. In between each task epoch, all the subjects were asked to perform an additional fatigue inducing task of moving a 1 kg mass in the sagittal plane in the same posture of ST and DT. Principal purpose of this task was to promote quick induction of fatigue in the respective muscle. This study was designed in consultation with eminent laparoscopic surgeons. A metronome reference was used to maintain the task uniformity for all the subjects. The recorded signals after the initial processing was considered for further analysis and validation.

4. Results and discussions

4.1. Characteristics of tremor at different task epoch

Throughout the experimental task, the accelerometers placed on the fore arm and the palm were used for calculating the values of respective joint angles. Fig. 4 shows the wrist and the elbow joint angle in sagittal plane of a subject while performing the dynamic line tracking task.

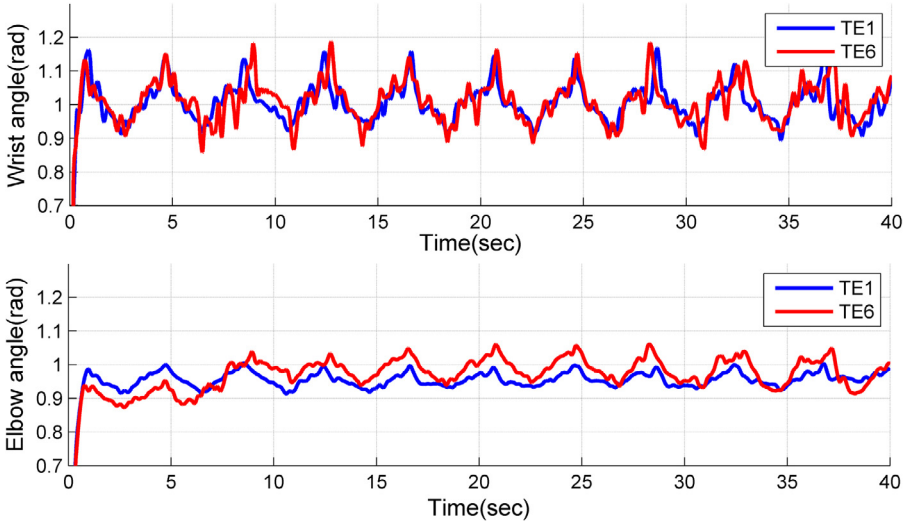

Fig. 4. Wrist and elbow angle plot at 1st and the 6th task epoch for the line tracking experiment.

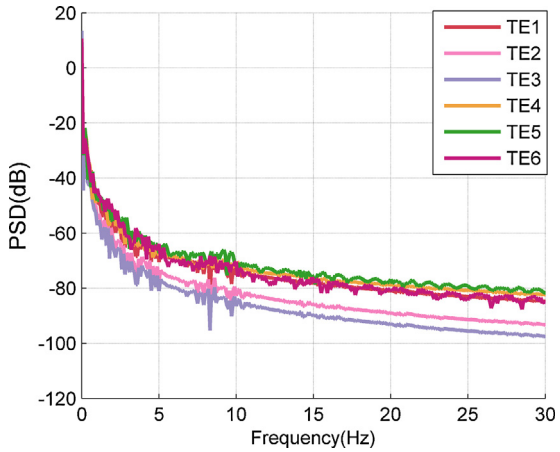

Fig. 5. PSD of the tremulous movement at each fatigue level.

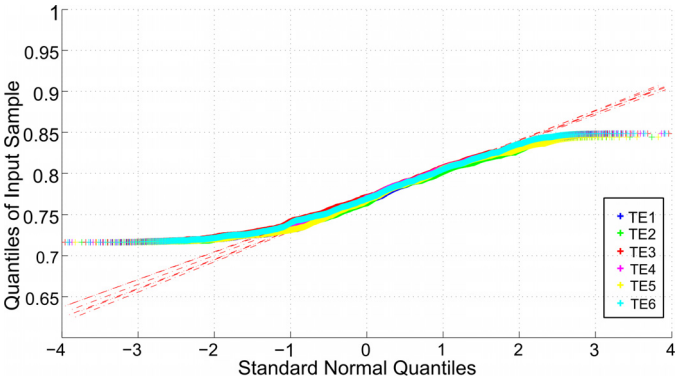

Fig. 6. Quantile–Quantile plot of elbow accelerometer value at each task epoch (TE).

It can be observed that with the elapsed time, the characteristics of the joint angle changes between first task epoch (TE-1) and sixth task epoch (TE-6), indicating the effect of the augmented tremor on the hand motion.

The wrist and the elbow joint values were used for calculating the trajectory of the tool grasping center. Variation in the frequency content of the tremulous trajectory data at different task epochs (TE-1 to TE-6) were captured by the Power Spectral Density (PSD) plot, as shown in Fig. 5. Though the intended motion was having a constant frequency, due to the change in the additive FIT with time, the signal frequency characteristics changes at different task epochs. In Fig. 5, PSD of the recorded signal shows a clear evidence of increment of the energy in the higher spectrum of the frequency content.

In the dynamic experimental task intended motion was having a frequency of 0.2 Hz, which is prominent as a high peak in the PSD plot. While the intended laparoscopic tool movement remains unchanged, additive high frequency tremor increases due to the increased level of muscle fatigue at the consecutive task epochs. Frequency axis of the PSD plot in Fig. 5 is limited to 30Hz following the significant fatigue induced hand tremor spectrum [36,37]. Major features visible in the plot are the peaks around 4 Hz, 8 Hz, and 16 Hz which is common for submaximal voluntary contraction. These peaks characterize the fatigue induced tremor. The frequency component between 8 Hz and 12 Hz is partially contributed by the physiological tremor as reported earlier [6]. An important feature of this plot is that with fatigue, high frequency component also increases. This difference attains a value as high as 20 dB at around 25 Hz.

Another significant aspect of the tremulous signal is it's nonstationary characteristics. The Quantile–Quantile plot in Fig. 6 depicts the sample quantiles of tremulous signal with respect to the theoretical quantiles from a reference normal distribution. The plot deviates at both end from the reference diagonal line which signifies that the FIT signal has an inherent nonlinearity. Even though the intended motion was repetitive in nature, this nonstationarity was imposed by the fatigue induced tremor which imposes variation in first moment (mean value) and the joint moment (autocorrelation) [16]. The intended LTM motion trajectory with adhered non-stationary hand tremor was used for EMD based compensation.

4.2. EMD, and IMFs of the laparoscopic tool trajectory

IMFs of the tremulous manoeuvering trajectory were calculated using the EMD framework. Fig. 7 shows the IMFs of an experimentally acquired FIT affected LTM data, the particular data was recorded at 4th task epoch (after 40 min).

The top most plot on the left is the main signal (original data), extracted IMFs after EMD are shown separately from IMF_1 to IMF_{13}. IMF frequency decreases with the increasing order of the IMF; i.e., IMF_1 conceives highest frequency content and IMF_{13} contains the lowest frequency among the IMF bunch. Along with the decreasing frequency, the amplitude of IMF increases with its increasing order. IMFs being a mean zero signal [12], zero crossing of the IMFs directly gives an idea of the frequency content. First few lower order IMFs containing high-frequency signal, correspond to the augmented FIT, whereas the low frequency intended motion is represented by rest of the higher order IMFs. As the muscle fatigue increases with time, the tremor also increases as discussed in Section 3.2. The increased tremor starts invading into the higher order IMFs and changes frequency content of the IMFs.

4.3. Properties of the tremulous signal IMF

Number of zero crossing indicates hierarchically decreasing frequency content of IMFs, and thus also substantiates that partial reconstruction is an obvious choice for using EMD as a filtering process. Fig. 8 shows the plot of number of zero crossing of the IMFs shown in Fig. 7.

The number of zero crossing comes down to a value of 1 at IMF_{13} which happens to be the final of the IMF bunch, whereas the number of zero crossing of the first IMF is highest [15]. Variation of IMF amplitude and frequency content together are captured in the probability distribution of the respective IMF as discussed in Section 2.5. Probability distribution based differentiation of two signals works even though the signal is non-stationary in nature [38]. This characteristic makes probability distribution a relevant qualifier for the IMFs irrespective of their stationarity.

Probability distributions of IMF_1, IMF_3, IMF_5 are elegantly captured by the normal distribution fit to their respective histograms shown in Fig. 9.

The figure depicts that the lower order IMFs that contains higher frequency and possess a different Probability distribution than that of the higher order IMFs, which predominantly contributes to the low frequency intended motion. This characteristic dissimilarity between each pair of IMF distributions was quantified with SKLD at each task epoch for all subjects.

4.4. SKLD based selection of reconstruction threshold

Disparity between each pair of consecutive IMFs were calculated in a hierarchical manner by exploiting SKLD values as described in Section 2.5. Disparities in the probability distribution at each stage of cumulative signal reconstruction were contributed by the IMF

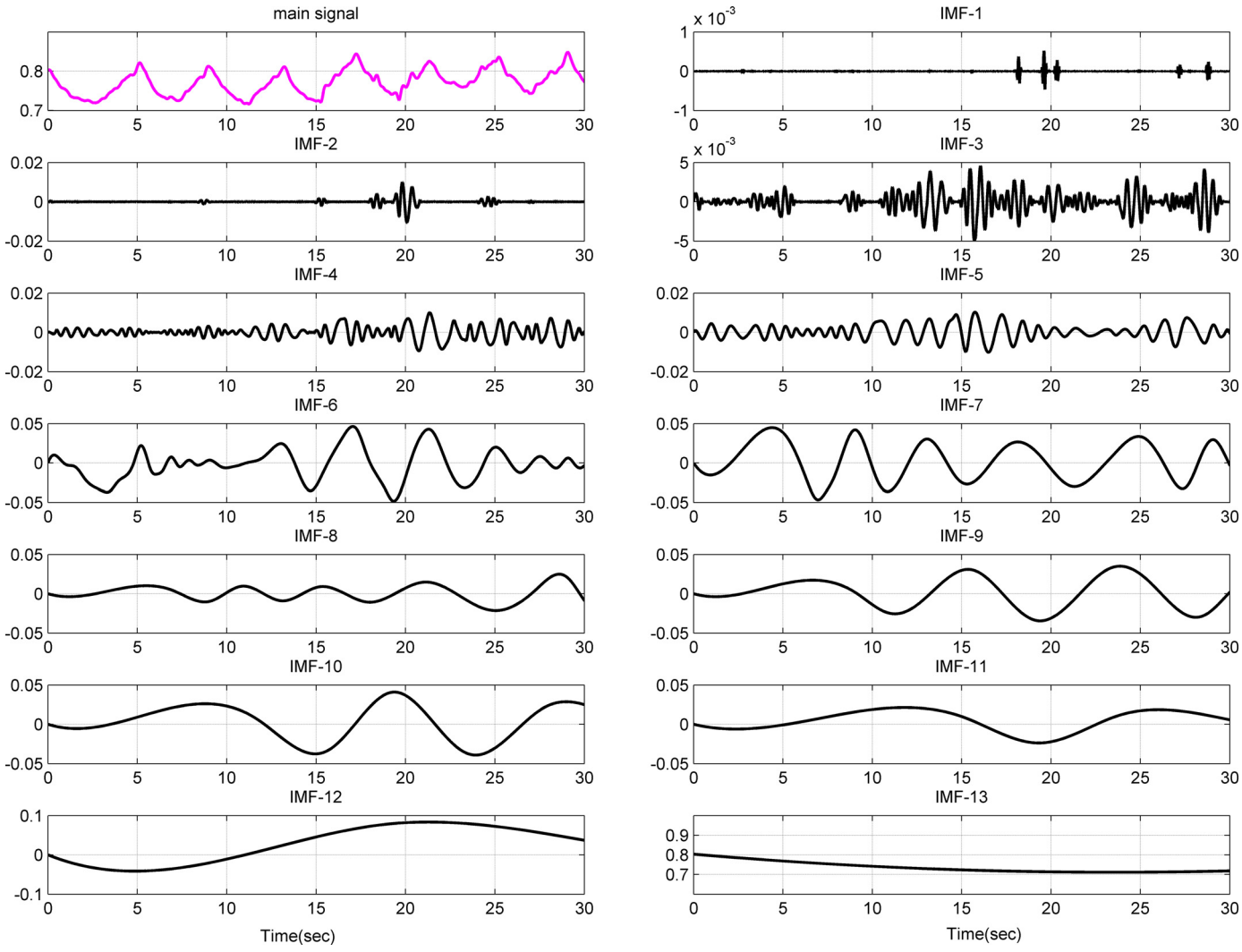

Fig. 7. Resolved IMF of the forearm accelerometer data (normalized), horizontal axis shows time (seconds).

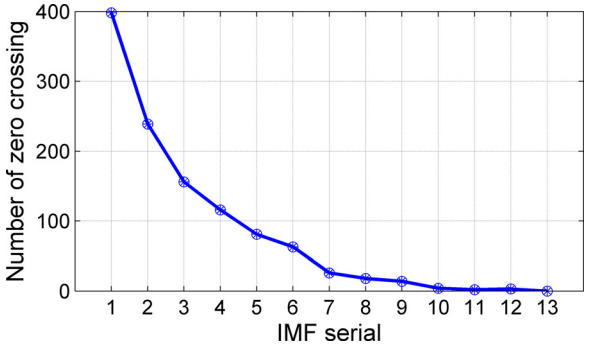

Fig. 8. Number of zero crossing for each respective IMF.

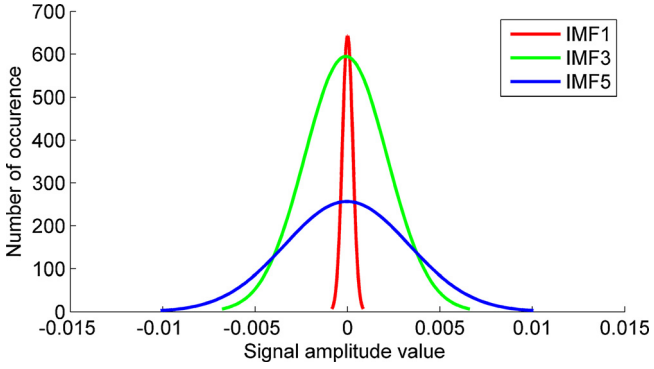

Fig. 9. Variation of IMF distribution shape.

of respective stage. After calculating all the SKLD among the IMFs, the maximum SKLD value (*max*(SKLD)) was considered as threshold for the partial reconstruction as given in (8). Fig. 10 shows the SKLD value among the consecutive IMF, for a particular signal the maximum attained SKLD value was found at $n = 6$. The *max*(SKLD) is located between IMF_6 and IMF_7 hence IMF_7 onwards were considered for the signal reconstruction whereas the lower order IMFs i.e. IMF_1-IMF_6 were discarded.

Efficacy of the proposed SKLD based separation of IMFs was investigated using synthetic as well as the experimentally acquired tremulous signal as discussed in the following section.

4.5. Signal reconstruction-simulation results with synthetic tremor-like signal

Intended motion and the unintended hand tremor had been studied in detail for surgeons [39,40]. It was reported that the

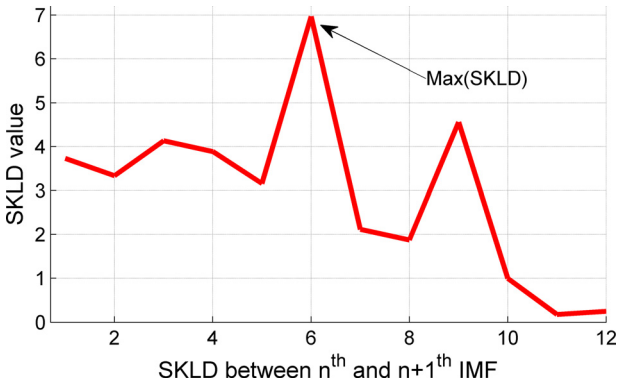

Fig. 10. Threshold IMF denoted by highest value of the SKLD.

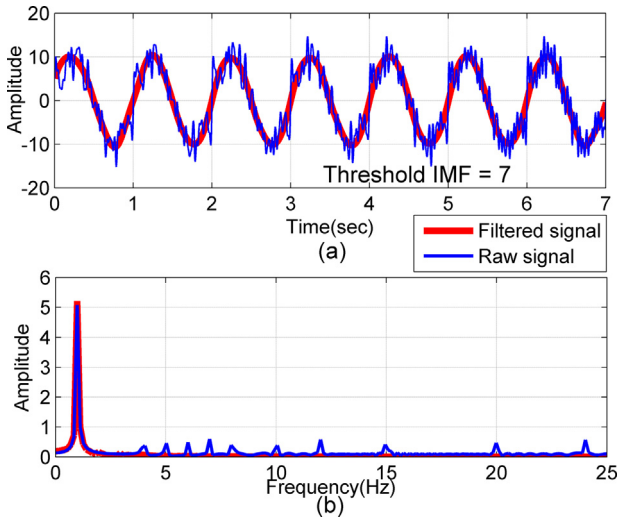

Fig. 11. Tremor compensated signal in time and frequency domain. (For interpretation of the references to color in text, the reader is referred to the web version of the article.)

frequency of the hand tremor varies between 4 Hz and 30 Hz, while the intended surgical motion frequency stays within 2 Hz [4,41,34]. EMD being a completely data driven process which has not been analytically described so far, we have extensively inspected for the $IMF_{threshold}$ and its variation with tremor-like synthetic signals. A low frequency sinusoid signal representing intended motion was artificially added with high frequency noise which represents FIT.

Fig. 11(a) shows a synthetic tremulous signal (blue color) and the FFT plot of the raw signal is shown in Fig. 11(b). The signal contains FIT alike higher frequency (4–24 Hz) along with the lower frequency intended motion. The $IMF_{threshold}$ was found to be IMF_7 and the filtered (red color) signal only contain the lower frequency signal which represents the intended motion. The filtering quality was also reflected in the frequency domain representation as Fig. 11(b) shows that the low frequency intended motion frequency content at 1 Hz was kept un-altered while the high frequency signals have been filtered out. This analysis was further extended for multiple tremor-like signals of varying frequency and amplitude in order to represent the time varying nature of additive higher frequency tremor in the signal. Here the contribution of different frequency contents in the synthetic signals were varied from a lower value (2 Hz) to a higher value (30 Hz) with 11 sets (C1–C11) as given in Table 1. In order to analyze the $IMF_{threshold}$, eleven different cases (R1–R11) have been chosen successively; in each case additional high frequency component has been introduced in a recursive manner and the threshold were calculated. In this

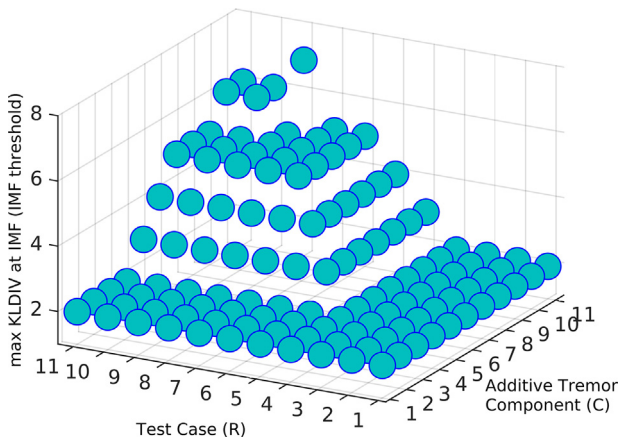

Fig. 12. IMF Thresholds for synthetic data with varying frequency and amplitude of additive tremor components.

process, the intended motion frequency (F_i) was considered to be less than 2 Hz. Simultaneously the amplitude of the synthetic tremor-like signals was gradually increased to a comparable level with the intended motion.

Amplitude and frequency of the synthetic signal that represents intended motion were kept unaltered as shown in the blue column of Table 1. The attributes of the high frequency tremor alike components were increased gradually imitating time varying additive FIT with intended motion. One relevant assumption was made in this scenario that there exist no signal frequency lower than the intended motion frequency, which is applicable as the tremor sensed at the joint angle always possess high frequency than the intended motion.

In each case the maximum SKLD representing the $IMF_{threshold}$ was calculated. The varying $IMF_{threshold}$ at each case was plotted with amplitude and frequency set in the other two axis as shown in Fig. 12. The $IMF_{threshold}$ was found to be increasing with the increasing frequency and amplitude content.

It is significant that the initial values of the $IMF_{threshold}$ stays within IMF_2 while it increases for the invoked higher frequency part. With the increment of high frequency component, the $IMF_{threshold}$ changes to higher values from IMF_2 to a highest value at IMF_7 at higher frequency, representing high tremor at increased fatigued level. It is necessary to have a clear idea about the threshold at different fatigue levels as the threshold changes at different level of muscle fatigue induced tremor.

4.6. $IMF_{threshold}$ *of experimental data at different task epoch*

Each task epochs resembles different tremor attribute due to increased muscle fatigue. In order to find out the $IMF_{threshold}$ at each stage, the experimental data were fed through the same threshold detection framework as discussed in Section 4.4. Fig. 13 shows the boxplot of $IMF_{threshold}$, along with the average mean BB-SEMG frequency for all the subjects at each task epoch.

The threshold was found to be increasing to a higher value with increasing fatigue level associated with increased tremor at consecutive task epochs. The results are coherent with the findings of the synthetic signals. Decreasing SEMG mean frequency values at different task epochs represents increasing fatigue [42]. For the 1st task epoch (TE-1), $IMF_{threshold}$ was found to be the 2nd IMF, while for TE-2, TE-3 and TE-4 this threshold changes to 3rd IMF. Finally at the TE-6 the threshold changes to 4th IMF. These changes of the threshold occur as the high frequency contents of the signal increases in the higher task epochs due to increased fatigue.

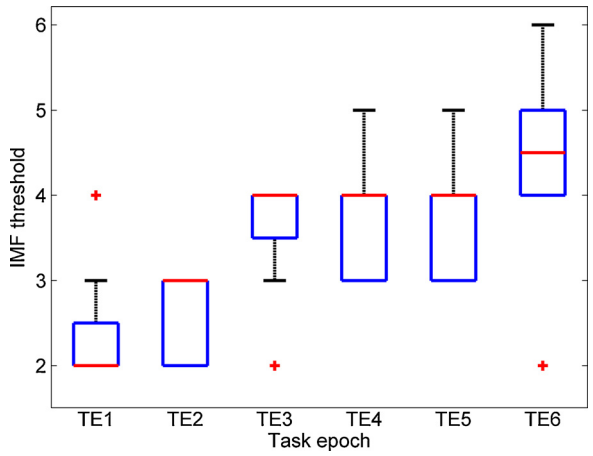

Fig. 13. Average IMF threshold and SEMG mean frequency for all the subject at each task epoch. The box-plot shows the median threshold value (red line), interquartile range and the red (+) marks denote the outliers in the IMF threshold values. (For interpretation of the references to color in this figure legend, the reader is referred to the web version of the article.)

Even though the subjective variations are reflected in the box-plot, it is clear that higher fatigue levels show a threshold trend on the higher side. In current work, the median values were rounded off to the nearest integer value for plausible calculation. These thresholds were finally selected for reconstructing the signal from the raw data.

4.7. Tremor filtering with partial reconstruction

Based on the $IMF_{threshold}$ values, the tremor filtering was performed at different task epoch for all the subjects. Fig. 14(a) and (b) shows the raw tremulous signal and the filtered signal at TE-1 and TE-6 for DT. Result shows a consistent performance of the proposed filtering approach in case of varying tremor characteristics at different task epochs. TE-1 and TE-6 represent two extreme case of induced muscle fatigue level, where resulting FIT has distinct characteristics. Effect of the FIT with the varying frequency was reduced while the intended motion was secured at all task epochs. A cross spectral correlation of the filtered and non-filtered signal substantiates the fact as shown in Fig. 14(c) and (d). The spectral coherence indicates the cross spectral density among the non-filtered and filtered signal at different frequency. The values indicate the magnitude squared coherence estimate of the signal before and after filtering.

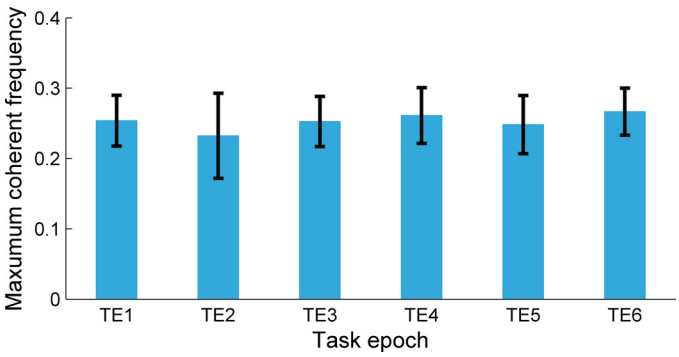

Fig. 15. Frequency value having highest correlation before after the filtering.

The highest correlation (correlation value = 1) among the filtered and the raw signal was found to be near 0.2 Hz frequency, which was the intended motion frequency of the instructed dynamic line tracking task. It confirms that non-filtered and filtered signal have the common component at 0.2 Hz. On the contrary, the high frequency portion of the signal shows a lower correlation than the intended motion frequency.

Highest correlation at intended motion frequency was found to have a slight variation, this was expected as normal subjective variation. Fig. 15 shows the maximum correlation frequency for all the subjects at different task epochs, the subjective variation is also shown with the error bar attached with the plot.

The highest correlation values signify the intended motion for all the cases. All these results together signify that the proposed method of minimizing the effect of tremor is highly effective in

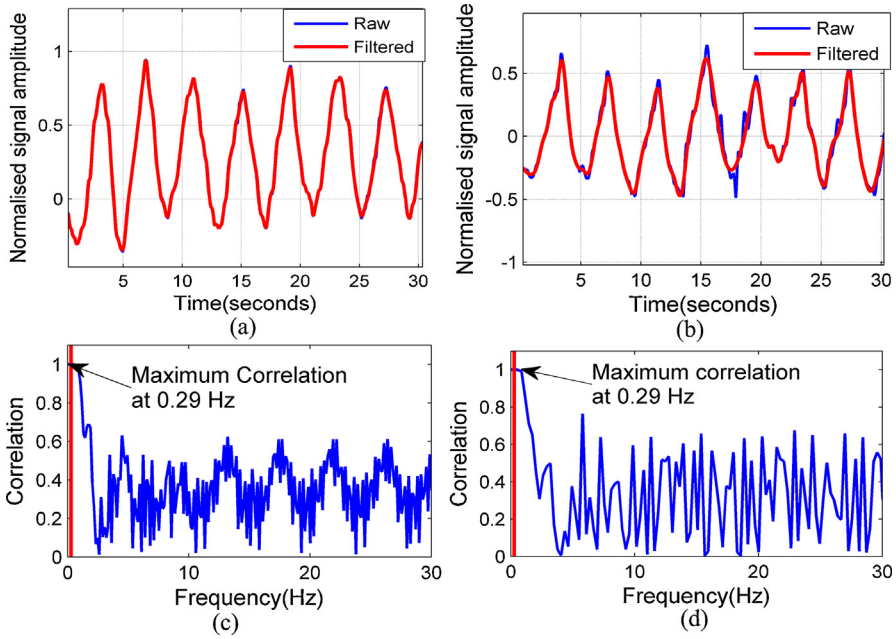

Fig. 14. (a) Raw and the filtered signal at TE-1, (b) raw and the filtered signal at TE-6, (c) spectral correlation among the raw and the filtered signal at TE-1, (d) spectral correlation among the raw and the filtered signal at TE-6.

Table 1
Amplitude (A) and frequency (F) set for synthesized signal, frequencies are in Hz. Blue column contains intended motion parameters (A_i, F_i), while the different additive tremor component parameters (A, F) are shown in other columns (C1–C11).

Test Case	Intended Motion		Additive Tremor Component																			
	C1		C2		C3		C4		C5		C6		C7		C8		C9		C10		C11	
	A_i	F_i	A	F	A	F	A	F	A	F	A	F	A	F	A	F	A	F	A	F	A	F
R1	10	1	0	0	1	5	0	0	0	0	0	0	0	0	0	0	0	0	0	0	0	0
R2	10	1	1	4	1	5	0	0	0	0	0	0	0	0	0	0	0	0	0	0	0	0
R3	10	1	2	4	1	5	1	6	0	0	0	0	0	0	0	0	0	0	0	0	0	0
R4	10	1	3	4	1	5	1	6	1	7	0	0	0	0	0	0	0	0	0	0	0	0
R5	10	1	4	4	1	5	1	6	1	7	1	8	0	0	0	0	0	0	0	0	0	0
R6	10	1	5	4	1	5	1	6	1	7	1	8	1	10	0	0	0	0	0	0	0	0
R7	10	1	6	4	1	5	1	6	1	7	1	8	1	10	1	12	0	0	0	0	0	0
R8	10	1	7	4	1	5	1	6	1	7	1	8	1	10	1	12	1	15	0	0	0	0
R9	10	1	8	4	1	5	1	6	1	7	1	8	1	10	1	12	1	15	1	20	0	0
R10	10	1	9	4	1	5	1	6	1	7	1	8	1	10	1	12	1	15	1	20	1	24
R11	10	1	9	4	1	5	1	6	1	7	1	8	1	10	1	12	1	15	1	20	1	24

LTM, even though the high frequency tremor changes depending on the time-variant muscle induced fatigue level.

5. Conclusions

In this paper an EMD based tremor compensation method was proposed and demonstrated in order to address the problem of minimizing the effect of the fatigue induced hand tremor in laparoscopic tool manipulation using the data driven EMD process. The inherent increased time resolution and superior data adaptability of this EMD based approach permits an improved signal handling despite the tremor signal is changing with induced muscle fatigue. Even though the mental fatigue state plays an important role, the experimental setup and protocol was designed such that the variations of tremor happens predominantly due to the muscle fatigue. The compensation scheme was limited within the dominant axis of muscle fatigue induced hand tremor. Reconstruction of the tremor free signal was successfully performed on tremulous signal at different level of increasing muscle fatigue. The compensation strategy has been validated with extensive synthetic and experimental data. The proposed method adapts the popular SKLD based inspection of IMF for differentiating tremor containing and no tremor containing IMF. This proposed method demonstrates for the first time that the fatigue induced tremor can be asymptotically reduced without distorting the intended motion. This method opens a new area of tremor compensation where the conventional fixed cut-off filters were unable to perform well. The current bottom up approach of sensing tremor from the joint spaces instead of the end effector space is a better way to estimate the individual contribution of tremor at each joint. For future work, we are preparing for the implementation for the experimental output for a robot assisted surgical system with a moving window based EMD process.

Acknowledgements

This work was supported jointly by Indian Institute of Technology Madras and European Commission (under Erasmus Mundus program). The work was carried out at LIRMM, France and Robotics Laboratory, Department of Engineering Design, Indian Institute of Technology Madras, India. We are thankful to Dr. M. Ramalingam from PSG Institute of Medical Science and Research for his support in framing the experimental protocol.

References

[1] L.S. Carreras, M. Hagen, R. Gassert, H. Bleuler, Survey on surgical instrument handle design: ergonomics and acceptance, Surg. Innov. 19 (50) (2011) 59.
[2] M. Silvennoinen, J. Mecklin, P. Saariluoma, T. Antikainen, Expertise and skill in minimally invasive surgery, Scand. J. Surg. 98 (4) (2009) 209–213.
[3] A. Hansen, R. Schlinkert, Hand movements in laparoscopic suturing: a simple vector analysis, Surg. Endosc. Other Interv. Tech. 19 (3) (2005) 412–417.
[4] J. Rosen, M. Macfarlane, C. Richards, B. Hannaford, M. Sinanan, Surgeon-tool force/torque signatures-evaluation of surgical skills in minimally invasive surgery, Surg. Endosc. Other Interv. Tech. 62 (1999) 290–296.
[5] P. Slack, X. Ma, Time dependency assessment of muscular fatigue index and hand tremor under operating conditions, in: 29th Annual International Conference of the EMBS 2007, IEEE, Lyon, 2007, pp. 4822–4825.
[6] O. Lippold, The tremor in fatigue, in: R.P.J. Whelan (Ed.), in: Ciba Foundation Symposium 82 – Human Muscle Fatigue: Physiological Mechanisms, vol. 1, John Wiley & Sons, Ltd., Chichester, 1981, pp. 234–248.
[7] B. Becker, R. MacLachlan, L. Lobes, G. Hager, C. Riviere, Vision-based control of a handheld surgical micromanipulator with virtual fixtures, IEEE Trans. Robot. 29 (3) (2013) 674–683.
[8] S. Chandra, M. Hayashibe, A. Thondiyath, Dominant component in muscle fatigue induced hand tremor during laparoscopic surgical manipulation, in: 36th Annual International Conference of the EMBS 2014, IEEE, Chicago, IL, 2014, pp. 6539–6542.
[9] E. de Lima, A. Andrade, J. Pons, P. Kyberd, S. Nasuto, Empirical mode decomposition: a novel technique for the study of tremor time series, Med. Biol. Eng. Comput. 44 (7) (2006) 569–582.
[10] A.O. Boudraa, J.C. Cexus, EMD-based signal filtering, IEEE Trans. Instrum. Meas. 56 (6) (2007) 2196–2202.
[11] J. Spyers-Ashby, P. Bain, S. Roberts, A comparison of fast Fourier transform (FFT) and autoregressive (AR) spectral estimation techniques for the analysis of tremor data, J. Neurosci. Methods 83 (1) (1998) 35–43.
[12] N.E. Huang, Introduction to the Hilbert–Huang transform and its related mathematical problems, in: Hilbert–Huang Transform and Its Applications, World Scientific, 2005, pp. 1–26 (Chapter 1).
[13] E.R. de Lima, A.O. Andrade, J.L. Pons, P. Kyberd, S.J. Nasuto, Empirical mode decomposition: a novel technique for the study of tremor time series, Med. Biol. Eng. Comput. 44 (7) (2006) 569–582.
[14] H. Xie, Z. Wang, Mean frequency derived via Hilbert–Huang transform with application to fatigue EMG signal analysis, Comput. Methods Prog. Biomed. 82 (2) (2006) 114–120.
[15] C. Junsheng, Y. Dejie, Y. Yu, Research on the intrinsic mode function (IMF) criterion in EMD method, Mech. Syst. Signal Process. 20 (4) (2006) 817–824.
[16] S. Chandra, M. Hayashibe, A. Thondiyath, Empirical mode analysis for characterization of hand tremor in the design of laparoscopic tools, ASME J. Med. Devices 9 (3) (2015) 030932.
[17] P. Flandrin, G. Rilling, P. Goncalves, Empirical mode decomposition as a filter bank, IEEE Signal Process. Lett. 11 (2) (2004) 112–114.
[18] Y. Kopsinis, S. McLaughlin, Development of EMD-based denoising methods inspired by wavelet thresholding, IEEE Trans. Signal Process. 57 (4) (2009) 1351–1362.
[19] S. Tabibian, A. Akbari, Noise reduction from speech signal based on wavelet transform and Kullback–Leibler divergence, in: International Symposium on Telecommunications, 2008. IST 2008, IEEE, Tehran, 2008, pp. 787–791.
[20] A. Komaty, A.O. Boudraa, B. Augier, D. Dare-Emzivat, EMD-based filtering using similarity measure between probability density functions of IMFs, IEEE Trans. Instrum. Meas. 63 (1) (2014) 27–34.

[21] R.M. Enoka, J. Duchateau, Muscle fatigue: what, why and how it influences muscle function, J. Physiol. (2008) 11–23.
[22] M. Knaflitz, P. Bonato, Time-frequency methods applied to muscle fatigue assessment during dynamic contractions, J. Electromyogr. Kinesiol. 9 (5) (1999) 337–350.
[23] J.Z. Liu, R.W. Brown, G.H. Yue, A dynamical model of muscle activation, fatigue, and recovery, Biophys. J. 82 (5) (2002) 2344–2359.
[24] R.N. Meeson, Introduction to the Hilbert–Huang transform and its related mathematical problems, in: Hilbert–Huang Transform and Its Applications, World Scientific, 2005, pp. 75–105 (Chapter 4).
[25] I. Nisky, M. Hsieh, A. Okamura, Uncontrolled manifold analysis of arm joint angle variability during robotic teleoperation and freehand movement of surgeons and novices, IEEE Trans. Biomed. Eng. 61 (12) (2014) 2869–2881.
[26] M. Alessandrini, A. De Padova, B. Napolitano, A. Camillo, E. Bruno, The AESOP robot system for video-assisted rigid endoscopic laryngosurgery, Eur. Arch. Oto-Rhino-Laryngol. 265 (9) (2008) 1121–1123.
[27] I. Nisky, S. Patil, M.H. Hsieh, A.M. Okamura, Kinematic analysis of motor performance in robot-assisted surgery: a preliminary study, in: Medicine Meets Virtual Reality, Studies in Health Technology and Information, vol. 184, 2013, pp. 302–308.
[28] C.G.L. Cao, C.L. Mackenzie, S. Payandeh, Task and motion analyses in endoscopic surgery, in: Proceedings of the 5th Annual Symposium on Haptic Interfaces for Virtual Environment and Teleoperator Systems, ASME, Atlanta, 1996, pp. 583–590.
[29] F. Bagala, V. Fuschillo, L. Chiari, A. Cappello, Calibrated 2D angular kinematics by single-axis accelerometers: from inverted pendulum to n-link chain, IEEE Sensor J. 12 (3) (2012) 479–486.
[30] S. Dyer, J. Dyer, Cubic-spline interpolation. 1, IEEE Instrum. Meas. Mag. 4 (1) (2001) 44–46.
[31] J. Zhang, B. Price, R. Adams, K. Burbank, T. Knaga, Detection of involuntary human hand motions using Empirical Mode Decomposition and Hilbert–Huang Transform, in: 51st Midwest Symposium on Circuits and Systems, 2008, Knoxville, 2008, pp. 157–160.
[32] T. Haidegger, B. Beny, L. Kovcs, Z. Beny, Force sensing and force control for surgical robot, in: Proceedings of the 7th IFAC Symposium on Modelling and Control in Biomedical Systems, vol. 1, International Federation of Automatic Control, Hus, 2009, pp. 413–418.
[33] R. Galleano, F. Carter, S. Brown, T. Frank, A. Cuschieri, Can armrests improve comfort and task performance in laparoscopic surgery? Ann. Surg. 243 (3) (2006) 329–333.
[34] I. Nisky, M. Hsieh, A. Okamura, A framework for analysis of surgeon arm posture variability in robot-assisted surgery, in: IEEE International Conference on Robotics and Automation (ICRA), Karlsruhe, 2013, pp. 245–251.
[35] F. Mobasser, J. Eklund, K. Hashtrudi-Zaad, Estimation of elbow-induced wrist force with EMG signals using fast orthogonal search, IEEE Trans. Biomed. Eng. 54 (4) (2007) 683–693.
[36] C. Riviere, W.T. Ang, P. Khosla, Toward active tremor canceling in handheld microsurgical instruments, IEEE Trans. Robot. Autom. 19 (5) (2003) 793–800.
[37] S. Morrison, J. Kavanagh, S. Obst, J. Irwin, L. Haseler, The effects of unilateral muscle fatigue on bilateral physiological tremor, Exp. Brain Res. 167 (4) (2005) 609–621.
[38] A. Mukherjee, A. Sengupta, Estimating the probability density function of a nonstationary non-Gaussian noise, IEEE Trans. Ind. Electron. 57 (4) (2010) 1429–1435.
[39] P.S. Slack, X. Ma, Tremor amplitude determination for use in clinical applications, Meas. Sci. Technol. 18 (11) (2007) 3471.
[40] J.A. Gallego, E. Rocon, J.O. Roa, J.C. Moreno, J.L. Pons, Real-time estimation of pathological tremor parameters from gyroscope data, Sensors 10 (3) (2010) 2129.
[41] V. Datta, S. Mackay, M. Mandalia, A. Darzi, The use of electromagnetic motion tracking analysis to objectively measure open surgical skill in the laboratory-based model1, J. Am. Coll. Surg. 193 (5) (2001) 479–485.
[42] S. Kattla, M.M. Lowery, Fatigue related changes in electromyographic coherence between synergistic hand muscles, Exp. Brain Res. 202 (1) (2010) 89–99.